Available online at www.sciencedirect.com
SCIENCE DIRECT
International Journal of Heat and Fluid Flow 27 (2006) 42–53
International Journal of HEAT AND FLUID FLOW
www.elsevier.com/locate/ijhff

Influence of hole imperfection on jet cross flow interaction

M.B. Jovanović *, H.C. de Lange, A.A. van Steenhoven

Technische Universiteit Eindhoven, Department of Mechanical Engineering, Division Thermo-Fluids Engineering, P.O. Box 513, 5600 MB Eindhoven, The Netherlands

Received 25 January 2005; received in revised form 10 June 2005; accepted 18 June 2005
Available online 11 October 2005

Abstract

The influence of a small hole geometry variation on the jet cross flow interaction is investigated experimentally using particle image velocimetry and liquid crystal thermography. The flow characteristics correspond to film cooling in gas turbines. A production imperfection is represented with the small variation of the hole geometry. The experiments were conducted without and with the hole imperfection at three velocity ratios. If the imperfection is absent, the flow field is stable and clockwise vortices are detected downstream. The imperfection blocks the hole, accelerates the jet and changes the formation of large vortical structures. It produces the additional windward vortices, which influence the flow field and enhance the inflow of the cross-stream towards the cooled surface. The imperfection reduces the film cooling effectiveness.

Keywords: Jet in cross flow; PIV; Film cooling; Flow structures; Effectiveness

1. Introduction

The study of a jet in cross flow is relevant to many engineering applications such as film cooling in gas turbines, fuel injection, smokestack pollution dispersion, V/STOL (vertical short take off and landing) aircraft control etc. Although similar characteristics can be found in all these flow fields, details can be quite different depending on many variables.

In this paper, we investigate a jet cross flow interaction with film cooling characteristics. Heat transfer is an important issue for the optimization and maintenance of gas turbines (Schook et al., 2001). Because of intensive heat transfer, gas turbine elements must be cooled. Film cooling is a method used in gas turbines to protect and cool blades, vanes and elements of a combustion chamber. The coolant is air extracted from a compressor and ejected through discrete holes and slots into an external boundary layer of gas turbine elements. Film cooling holes in turbine blades have been mostly produced with electro discharge and electro chemical drilling. Nowadays, application of laser drilling is increasing. A laser drilling process is faster but also cruder. Imperfections in a hole may reach even 25% of a hole diameter. Therefore, a detailed study is needed to investigate the influence of a hole production imperfection on film cooling.

The jet cross flow (JCF) interaction has been widely investigated. One of the first detailed papers which report the transverse jet in the cross flow was written by Bergeles et al. (1976). They detected the shift of the jet velocity profile towards the lee side. Turbulence characteristics of an isolated normal jet in cross flow were reported by Andreopoulos and Rodi (1984). Moussa et al. (1997) studied the mixing of the JCF. Smith and Mungal (1998) investigated mixing structure and scaling. Peterson and Plesniak (2002) examined the influence of the supply plenum configuration. Averaged results of the flow field in all three planes were presented. They found that the plenum feed direction has an influence on the flow field. Elliptic jets were investigated by New et al. (2003). Haven and Kurosaka (1997) proved that the inlet geometry of the film cooling hole

* Corresponding author. Tel.: +31 40 247 2877; fax: +31 40 243 3445.
E-mail address: m.jovanovic@tue.nl (M.B. Jovanović).

0142-727X/$ - see front matter © 2005 Elsevier Inc. All rights reserved.
doi:10.1016/j.ijheatfluidflow.2005.06.003

Nomenclature

D	hole diameter
U_∞	cross-flow velocity
V_j	jet velocity
A_j	surface of the hole cross-section
ρ_j	jet density
ρ_∞	cross flow density
δ	boundary layer thickness
δ^*	boundary layer displacement thickness
η	film cooling effectiveness

Normalized variables

Re_x	Reynolds number related to the distance from the plate leading edge till the hole leading edge
Re_D	Reynolds number related to the hole diameter
MR	mass flux ratio
VR	velocity ratio
X	normalized streamwise coordinate $X = x/D$
Y	normalized coordinate perpendicular to the wall $Y = y/D$
Z	normalized spanwise coordinate $Z = z/D$
U, V, W	normalized components of a velocity in X, Y and Z directions respectively
Tu	turbulence intensity
Tu_u, Tu_v, Tu_w	turbulence intensity components in X, Y and Z directions

Abbreviations

Pi	perfect case in the ith case $i = 1, 2, 3$ (see Table 1)
ITi	inner-torus case in the ith case $i = 1, 2, 3$ (see Table 1)
PV	positive vortex
WV	windward vortex
LV	lee vortex
CVP	counter rotating vortex pair
JCF	jet cross flow interaction
LE	leading edge
TE	trailing edge

plays a significant role on the development of flow structures. Johnston et al. (2002) showed that the inlet geometry changes significantly the near flow field and does not have a large influence on the far field. Morton and Ibbetson (1996) analyzed the warp mechanism of the vortical structures. Fric and Roshko (1994) studied experimentally vortical structures in the wake of the transverse jet. Kelso et al. (1996) investigated experimentally the vortical structures in the jet cross flow interaction. The genesis and development of a counter rotating vortex pair was very well explained by Lim et al. (2001). The JCF was studied numerically by Yuan et al. (1999).

From literature it can be concluded that development of large vortical structures in the JCF depends on a mass flux ratio ($\mathrm{MR} = \frac{\int \rho_j V_j \, \mathrm{d}A_j}{\rho_\infty U_\infty A_j}$), For the MR < 2, which is the property of film cooling, four types of large vortical structures are detected (Fig. 1): A Counter rotating vortex pair (CVP), horseshoe vortex (HSV), windward (WV) and lee vortex (LV). The HSV forms in a similar way as in the flow around a blunt body. The pressure difference arises on the jet boundary and drives a vortex roll. When the jet is ejected in a steady surrounding the toroidal vortex is formed. If the jet is exposed to the cross flow the torodial vortex breaks and the WV and LV are formed (for more see Lim et al. (2001)). The ejected jet separates over the surface, and downstream of the hole it rolls and breaks to turbulence. The region behind the film cooling hole will be named here as the cooled volume. The presence of a bend in the JCF actuates a formation of the CVP. If we imagine the jet boundary to be nonporous, the system would consist of the hole, jet curvature and cooled volume. When the fluid particle enters the curvature it is exposed to the centrifugal force. This force is bounded for the windward side. In the same time the fluid particles around the axis of the curvature have the highest velocity which means that they are exposed to the highest centrifugal force. Under the influence of this force fluid particles, in the vicinity of the central line, move toward the windward side. To satisfy the continuity the particles with the smaller velocity, near the jet boundary, start to move to the lee side. This mechanism leads to the formation known as the CVP.

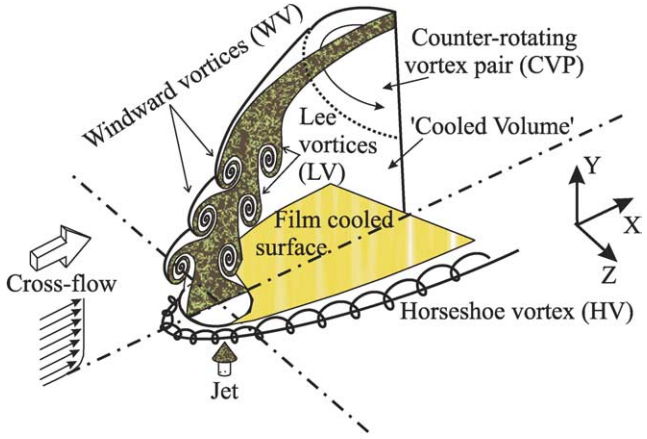

Fig. 1. Vortical structures in the jet cross flow interaction (JCF) with film cooling characteristics.

In the coming sections we will discuss how the vortical structures in the JCF are influenced by the imperfection inside the film cooling hole. The emphasis will be put on the formation of the vortical structures, their merging, advection and influence on the flow field and film cooling

effectiveness. To that end, first the experimental set up will be described in the Section 2. The averaged flow field will be presented and analyzed in Section 3. Although, the averaged data are very important, to understand the physics and behavior of vortical structures instantaneous flow fields must be analyzed (see Lourenco et al., 1997). Instantaneous data with the vortical structure behavior will be discussed in Section 4. The paper is concluded with experimental results of the film cooling effectiveness, which are presented in Section 4.3.

2. Experimental apparatus and procedure

2.1. Apparatus

The experiments were performed in a closed-return water channel at the Technische Universiteit Eindhoven (Eindhoven University of Technology). The water channel consists of two reservoirs and a closed test section. Incoming and outgoing reservoirs have been connected with three pipes and with the closed test section made of glass. The test section has a length of 3170 mm, a width of 600 mm and a height 450 mm. Because the walls of the test section are transparent, optical measurements can be conducted. The optical accessible volume in the test section is the volume of a cuboid with dimensions $2000 \times 550 \times 400$ mm. To obtain a water flow with a uniform velocity, a pair of flow straighteners was placed at the beginning of the test section. The flow straightener consists of rectangular combs (with a characteristic rectangle 6.1×5.2 mm) and a metal mesh (with a characteristic dimension 1.5 mm). This combination provides uniform flow with a turbulent intensity lower than 1% in the test section. Streaming energy is supplied with three pumps fed from the incoming reservoir. The speed inside the test section can be varied from 0 till 0.35 m/s.

Table 1
Experimental parameters

	U_∞ (mm/s)	$Re_x \times 10^{-5}$	δ/D	δ^*/D	(Perfect) VR	(Inner-Torus) VR
1	120	1.7	0.30	0.090	(P1) 0.54	(IT1) 0.92
2	190	2.7	0.21	0.072	(P2) 0.34	(IT2) 0.58
3	330	4.7	0.16	0.055	(P3) 0.20	(IT3) 0.33

2.2. Experiments

In the experiments a flat plate (1900×565 mm) made of Plexiglas was placed in the test section. The leading edge of the flat plate was at 600 mm from the flow-straightener. Below the leading edge an array of suction holes was made on the bottom of the test section to prevent separation at the leading edge. The scaling of the set-up is based on the corresponding Reynolds numbers and the boundary layer thickness (see Table 1). Due to the set-up limitation, the blowing ratio was varied changing the cross flow velocity. The boundary layer thickness was changed slightly, relative to the hole diameter. Hay et al. (1985) reported that the condition of the approach boundary layer makes hardly any difference to the heat transfer coefficient under the film. Bearing that in mind and taking in account that the Re_x was of the same order of magnitude in all three cases it was concluded that the model is sufficiently good to study and compare the jet cross flow interaction in different cases.

The jet was injected perpendicularly into the cross flow through the cylindrical hole with a diameter $D = 64$ mm (Fig. 2(A)). The cylinder was placed below the flat plate along the central line 1420 mm from the leading edge. The jet water supply consisted of a 450 l tank, pump and two hoses. The hoses were connected to a small plenum located below the jet hole. Inside the hole a small flow-straightener was implemented to suppress large turbulent structures. Due to geometric restrictions a short hole was

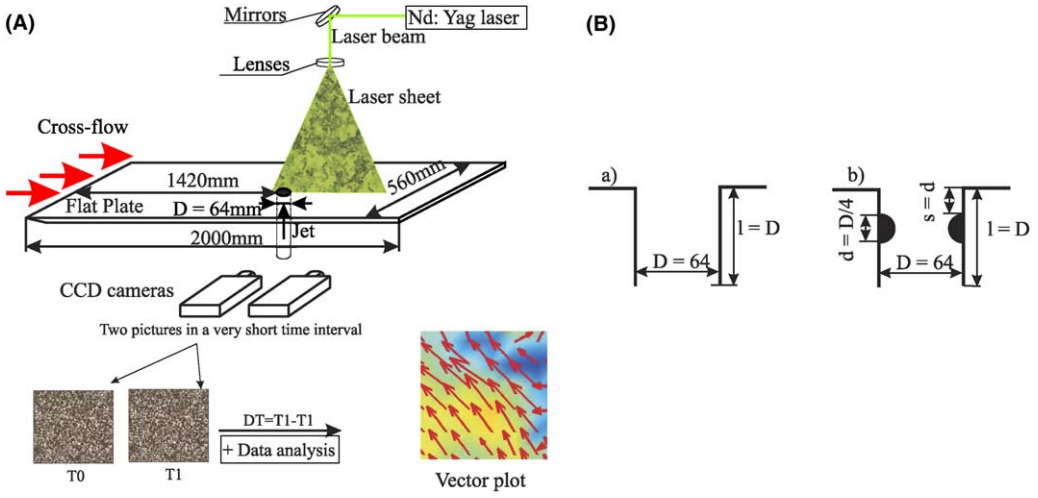

Fig. 2. (A) Set-up configuration for the vertical PIV measurements. (B) Geometry of the hole used in experiments: (a) The perfect hole, (b) The hole with the torus imperfection.

used; the length (l) over the diameter of the hole was 1. Two cases were investigated: the perfect (P) and inner-torus (IT) case. In the perfect case the jet was injected through the hole without any imperfections. We assumed that the production imperfection has the shape as a melt ejection (see van Allmen and Blatter, 1995). Therefore, a half torus was chosen to simulate the imperfection. During the drilling process an imperfection can occur anywhere in the hole. For purpose of this research the half torus was placed one torus diameter inside the hole in the IT case (Fig. 2(B)). The torus diameter was 16 mm ($d = D/4$). This is of the same order of magnitude as the imperfection produced during the drilling process.

The mass flow rate was constant. The averaged velocity of the jet in the plane of symmetry at the hole exit was 65 mm/s in the perfect case whereas in the inner-torus case it was 110 mm/s. The Reynolds number, based on the diameter Re_D was 4.2×10^3 and 7.0×10^3 at the hole exit.

2.3. Measurement techniques

Flow field measurements were done by means of Particle Image Velocimetry (PIV). As tracers, 20 μm polyamid seeding particles were used. A dual-pulse Nd:Yag laser ($\lambda = 532$ nm) was used to illuminate tracers. To form a 2 mm thick laser sheet (Fig. 2(A)), a negative lens and rectangular diaphragm were used. Images of the light reflected off particle surfaces were taken with CCD cameras (Kodak Megaplus 1008×1018 pixels, 10 bits) and the images were digitally stored on hard disks using the acquisition software VideoSavant. The sampling frequency was 15 Hz, which was limited by the Nd:Yag laser. PIV software, used to process the data, was developed at the Technische Universiteit Eindhoven. The software uses a standard algorithm to cross-correlate particle images in interrogation areas with sub-pixel interpolation (van der Plas and Bastiaans, 1998).

The PIV measurements were conducted in vertical and horizontal planes. Measurements in the vertical plane were carried out along the central line of the flat plate with two CCD cameras. The first camera was used to record the flow field above the hole while the second recorded the downstream flow field. The measurement field of one camera was 200×200 mm. Because of the low resolution the flow field was zoomed around the hole. The measurement field of one camera was reduced to 80×80 mm. Also vertical measurements out of the central plane were conducted. The horizontal measurements were conducted with one camera. The horizontal plane was located 33 mm above the plate surface. The average flow field and other statistical results were obtained by averaging and processing 250 frame pairs per measurement. Vortices in a flow field were detected using the Reynolds decomposition (for more see Adrian et al. (2000)). The measurements taken with two CCD cameras were processed and interlocked slightly behind the holes center. Therefore, a small discontinuity is detected in the zoomed measurements. The interrogation window was 32×32 pixels with an overlap of 50%. The uncertainty in the peak-finding algorithm is estimated to be 0.1 pixels, which gives the error in the velocity measurement between 1% and 2%.

Liquid crystal thermography (LCT) was used to measure temperature on the wall. To obtain these measurements coated polyester sheets of thermochromic liquid crystals were fixed on the plate. The thermochromic liquid crystals sheets have been produced by Hallcrest (type: R20C5W). The red starts at 20° and the bandwidth is 5 °C. The temperature in the channel was fixed at 20 °C and the jet temperature at the 26 °C. Instantaneous images were taken with a digital camera (Fujifilm FinePix S602 ZOOM) in the TIF format with a maximal resolution of 2832×2128. The calibration was conducted in situ by heating the water in the channel. The camera and light source were in the same position during the measurement and calibration process. The error was estimated on 0.2 ° Celsius. Since, the conductivity coefficient of the plexiglas is low, the plate surface can be treated as an adiabatic wall. Therefore, the effectiveness (η) can be calculated from the temperature measurements as:

$$\eta = \frac{T_\infty - T_{\text{wall}}}{T_\infty - T_{\text{jet}}}$$

Jet and cross flow temperature was constant and homogeneously distributed and it was measured with the mercury thermometer with the accuracy of 0.05 °C. Therefore, the absolute effectiveness error is 0.035.

2.4. Way of comparison

In this paper results are presented comparing the P and IT case. If the $\rho_j = \rho_\infty$ and $\int V_j \, dA = \overline{V}_j A_j$ than the MR is equal to the velocity ratio ($\text{VR} = \overline{V}_j / U_\infty$). A_j is the surface of the hole exit cross-section. In the P case cross-sections along the hole are constant and equal to A_j. In the IT case the torus blocks partially the hole, changes the cross-section and accelerates the velocity. Due to this acceleration the VR in the central plane is changed although the MR is the same as in the P case. The question is whether the cases with the same MR or central plane VR should be compared. In gas turbines the film cooling flow is driven by the pressure difference inside a blade and on its surface. Then the velocity must be constant and the mass flux is defined by means of the smallest cross-section. If this is true then the P and IT case need to be compared at the same VR. But Gritsch et al. (1998) reported the influence of a hole shape on a discharged coefficient ($C_D = \dot{m}_{\text{real}} / \dot{m}_{\text{ideal}}$). From their work, it is obvious that the mass flow is not a simple function of the cross-section. Therefore, we decided that P1 (the P case with the $\text{VR} = 0.54$) is going to be a bench mark in this paper. The bench mark is compared with IT1 (the same MR) and IT2 (the similar central plane VR). In the following text with the VR the central plane velocity ratio will be denoted.

3. Average data

3.1. Mean velocity profiles

In the short hole ($L/D < 2$) the jet profile cannot fully develop. Therefore, some jet properties are analyzed. All values are normalized with the hole diameter D and the cross flow velocity U_∞. The hole is short and the jet profile is not developed. Two peaks are detected in the perfect case. The inner-torus accelerates the jet and it smooths the jet profile. The jet is turbulent and vortical structures are irregular with a small length scale. The turbulence intensity of the jet is 10%. Pulsations of the jet are not detected.

When the cross flow is superimposed the jet profile changes drastically and the peaks move towards the lee side (see Fig. 3(B)). This was also reported by Bergeles et al. (1976) and Andreopoulos (1982) although they investigated a totally developed jet profile and hence detected only one peak at the lee side. At the exit of the hole the

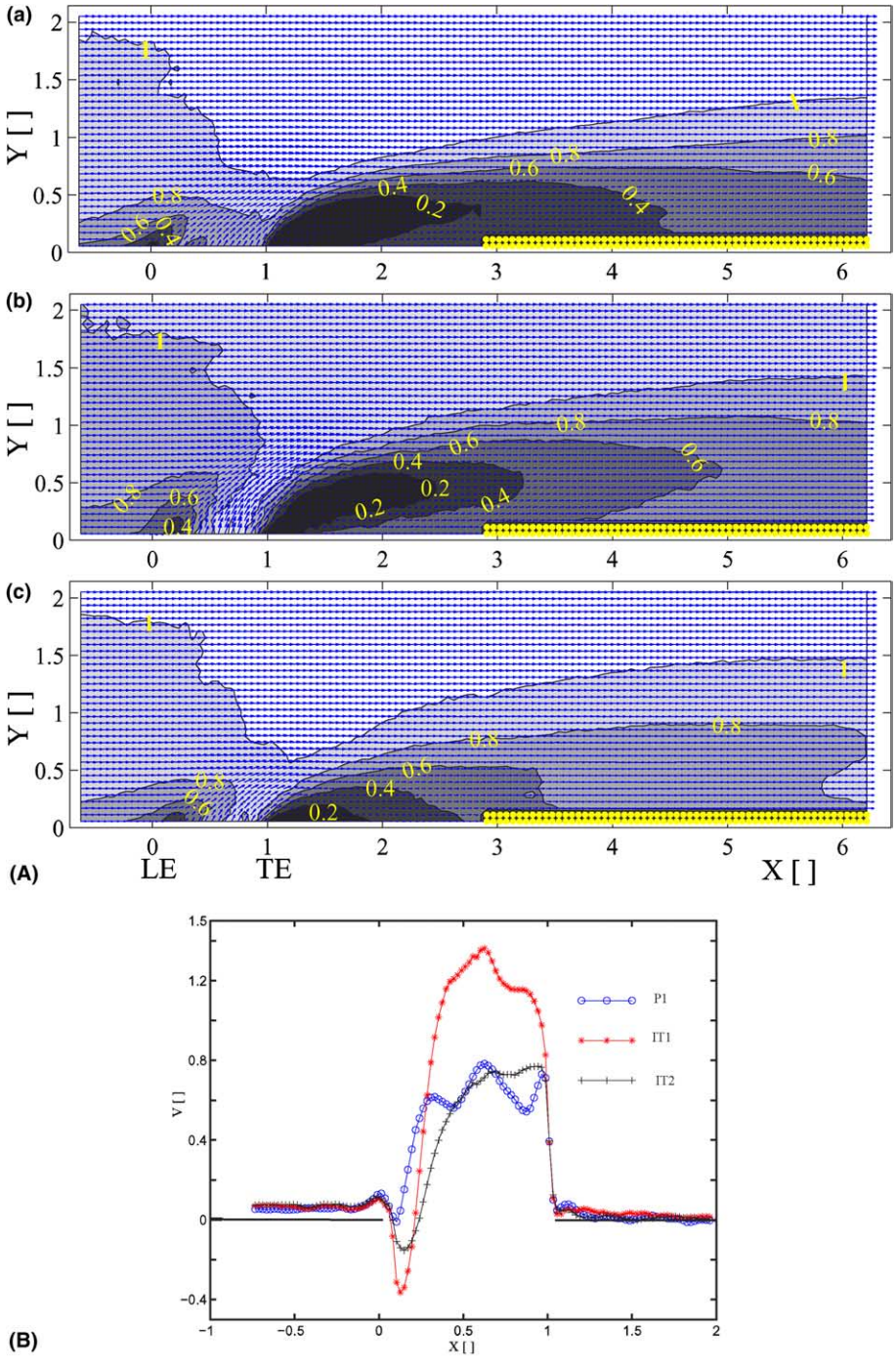

Fig. 3. (A) Averaged velocity field along the central plane: (a) The P1, (b) IT1 and (c) IT2 case. LE and TE denote the leading and trailing edge position. (B) V velocity profiles of the jet in P1, IT1 and IT2 at the hole exit.

V profile is flatter in IT2 than in P1. Further away from the hole exit, above 1.2 ($Y/D > 1.2$) all profiles are similar and they become almost flat with a slightly negative velocity. This negative velocity is a result of the accelerated cross flow above the hole. The cross flow penetrates the hole behind the leading edge. This penetration is small and rather constant in the P case and it does not depend on the VR. It is important to notice this small ingestion because it influences the formation of a vortical structure, which is explained in Section 4.1. In the IT case the ingestion of the cross flow is much more pronounced. The negative velocity is much higher than in the P case and it depends strongly on the VR (see Fig. 3(B) above $X = 0.1$).

3.2. Averaged velocity field

The averaged velocity fields are shown in Fig. 3(A) (white dots in this figure indicate region without data). Two shear layers are detected in all cases above and behind the film cooling hole. In the P case, the first shear layer starts in front of the leading edge. Part of the boundary layer lifts up with the jet but the other part penetrates the hole. The point, where the lift starts, is not effected by the VR but the shear layer angle decreases when the VR is decreased. The shape and lifting point of this shear layer are influenced by the inner-torus. The lift starts abruptly above the hole in the IT cases. The reason for this change is a higher ingestion of the boundary layer in the IT than in P case. This ingestion stabilizes the boundary layer but mixes a large amount of the hot fluid with the coolant already in the hole.

A second shear layer with fairly strong velocity gradients can be seen behind the trailing edge. This shear layer connects the cooled volume and free-stream. The influence of the jet is not present above 1.2 ($Y/D > 1.2$), which is in agreement with the results from V velocity profiles. The second shear layer starts at the trailing edge and spreads out. The start point is always at the hole trailing edge. The velocity gradient is smaller in P1 than in IT2.

In the cooled volume of P1 and IT1 a higher speed region is detected on the plate $0.5D$ behind the trailing edge. This region is absent in the IT2 and other cases. In the cooled volume near the plate surface the pressure is lower than in the free-stream. This enables the cross-fluid to penetrate the cooled volume close behind the hole. This inflow enhances the momentum and accelerates the flow near the surface. In IT2 the VR is even slightly higher than in the P1. But the influence of the gap, between the inner-torus and the exit of the hole, has the same effect on the flow as a shaped-hole. It retards the jet and the attachment of the coolant fluid to the plate surface is enabled. This prevents the cross flow penetration towards the central plane.

3.3. Turbulence intensity and kinetic energy–Tu

A high turbulence intensity (Tu) is detected above and downstream of the hole. Since the cross flow and the jet have the lower Tu, the reason for the higher Tu must be the interaction between the detached boundary layer on the flat plate and the separated region of the coolant flow. In P1 Tu_u is 18% ($Tu_u = 100\sqrt{\overline{u^2}}/U_\infty$) in front of and above the leading edge of the hole. The main contribution stems from the interaction of the boundary layer separation and the jet shear layer. At the higher cross flow rate, Tu_u in this region becomes smaller. $Tu_v = 100\sqrt{\overline{v^2}}/U_\infty$ in the P case is negligible. In the IT case the situation is qualitatively similar. Tu_v is rather small above and in front of the hole leading edge but Tu_u exceeds 30% in IT1, drops to 30% in IT2 and still is significant in IT3. The highest Tu_u in the P cases is above the leading edge while in the IT cases it is above the imperfection.

Behind the hole Tu_u and Tu_v have a similar contribution. The value of Tu_u reaches 30% in P1 and P2 in the region where the second shear layer is detected. In IT1 and IT2 Tu_u exceeds 30% and covers the whole cooled volume. Behind the trailing edge large fluctuations are generated due to the separation of the coolant flow. In the cooled volume, behind the trailing edge, the averaged velocity is zero, but the Tu is quite large. This could indicate a turbulent 'bounded' flow, which 'oscillates' between the second shear layer and the flat plate. This will be further discussed in Section 4.2.

A normalized two dimensional turbulent kinetic energy $k = \frac{1}{2}(u^2 + v^2)/U_\infty^2$ is presented in Fig. 4. Above the hole in the P1 case the region with the higher turbulence kinetic energy is found. This is likely due to the jet separation and the jet velocity gradient. The highest turbulence kinetic energy is detected in the second shear layer region and it decreases gradually from 7×10^{-2} over 5×10^{-2} to 2.5×10^{-2} for P1, P2 and P3 respectively.

In the IT cases the highest turbulence production is above the imperfection and the turbulent kinetic energy reaches 20×10^{-2} in IT1. This is 7 times larger than in P1 above the hole, while in the second shear layer region energy is twice as large as in P1. In IT2 energy is 6×10^{-2} (2 times more than in P1) above the hole and 9×10^{-2} (1.5 times more than in P1) in the second shear layer region. In the IT cases the turbulence production is quite significant above the hole where the turbulence kinetic energy is always higher than in the P cases.

4. Instantaneous data

4.1. Perfect hole

The instantaneous velocity fields in the perfect case are characterized by means of the quasi regular process. In Fig. 5 the typical instantaneous flow field in P1 is presented. At the windward side the vortical structures are not detected. At the lee side a large vortex can be seen. The mechanism, extracted from the row of the instantaneous data, can be described as separation over the trailing edge of the hole. The jet separates on the hole trailing edge

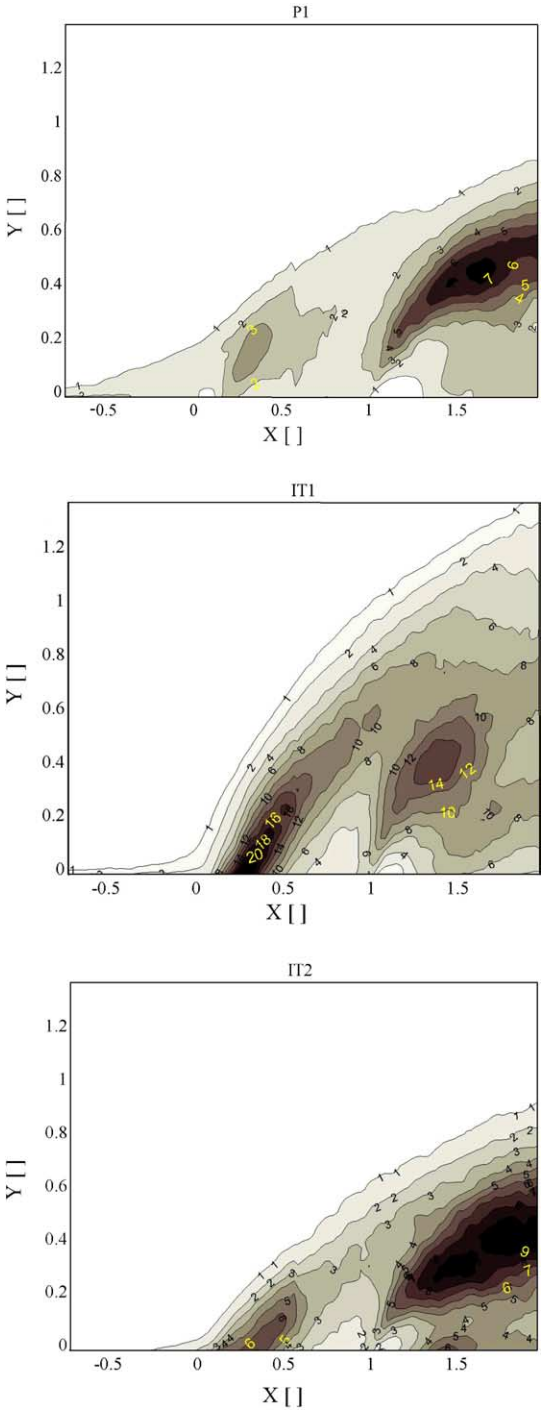

Fig. 4. Turbulent energy calculated with two velocity components along the central line $K_{uv}^2 = \frac{1}{2}(u^2 + v^2)/U_\infty^2$.

and rolls up at the lee side. Vortices grow and merge above the trailing edge. When they reach a certain size, they leave the surface of the plate and shed the second shear layer. The separation above the trailing edge has a high frequency. Once when a large vortical structure is distinguished in a flow field the tracking is possible. Most of the time in the central plane flow field, only the large vortical structures with the negative vorticity are detected.

In the averaged flow field (see Section 3) a region with high *Tu* and zero averaged velocity is detected at the lee side. This could lead us to assume that a stagnant bubble is generated. From the visualized instantaneous flow fields can be concluded that the stagnant bubble does not exist and the cooling process is influenced by separation over the trailing edge.

It is concluded that the interaction between the cross flow boundary layer and the jet does not produce large vortical structures at the windward side. A large vortical structure is detected downstream and can be seen in Fig. 5. The toroidal vortex of a free jet, which is inevitable when the jet is ejected in a steady surrounding, does not exist in the jet cross flow interaction at the low VRs.

4.2. Hole with the inner-torus

Fig. 6 presents three instantaneous flow fields in IT1. In Fig. 6(a) a few positive vortices are detected above the hole. At the lee side negative vortices are visible as they shed the second shear layer. A positive vortex, marked as PV, stands out $0.25D$ from the leading edge. This vortex is traceable and it is detected 0.33 and also 0.6 s later in Fig. 6(b) and (c). The shedding frequency of negative vortices, at the trailing edge, is higher and it is not possible to reconstruct totally the genesis of the negative vortex. Negative vortices are detected in all instantaneous fields with some variations. Additional positive vortex can be seen in Fig. 6(b) and (c) at the lee side. The appearance of these positive vortices at the lee side is not regular.

The genesis of large vortical structures is different in the IT and P cases. The separation starts already in the hole. The jet separates on the torus and produces a toroidal vortex. The toroidal vortex tends to leave the hole. The cross flow, which penetrates the hole, mixes with the coolant in the hole and breaks the toroidal vortex. The PV warps above the imperfection and enlarges inside the hole. When the PV reaches critical size it leaves the hole and sheds the first shear layer. This PV is a cross cut of a three dimensional windward vortex (WV). At the moment when the PV leaves the hole the cross flow penetrates the hole again, blocks partially the exit and presses the jet towards the plate wall.

The flow field is more chaotic at the lee side. The jet and a part of the toroidal vortex separate on the trailing edge. Due to this separation many smaller vortices are generated. They merge and form the bigger vortical structure, which sheds the second shear layer. These negative vortices are a cross-section along the central line of a three dimensional lee vortex (LV). In Fig. 6(c) the PV meets the negative vortex $1.25D$ downstream and they form a vortex pair.

Fig. 7(a) shows positive vortices: a PV1 and PV2. The PV1 sheds the first shear layer while PV2 grows attached to the plate surface till it reaches the same length scale as the scale of the cooled volume. In Fig. 7(b) PV1 and PV2 merge and lead us to the second scenario. When the jet is pushed down the negative vortex starts to warp on the

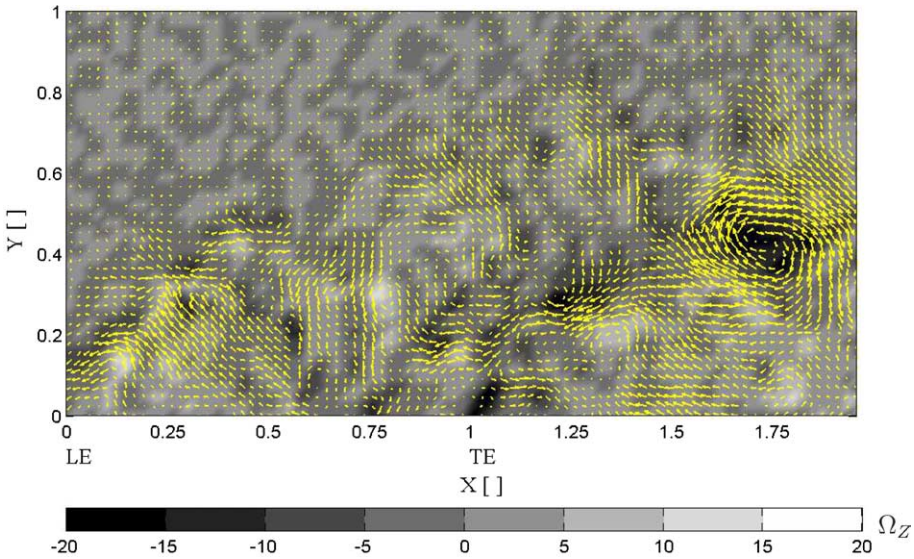

Fig. 5. The fluctuation field with vortical structures in P1. Vectors represent fluctuation velocity obtained using Reynolds decomposition. Vorticity is printed in the background.

plate wall. In the cooled volume the flow is blocked by the negative vortex. As a reaction on this action the positive vortex starts to roll. This positive reaction vortex is nothing else but the PV2 in Fig. 7(a). If the WV, instead of merging with the LV, joins the positive reaction vortex the flow field becomes highly disturbed. Thanks to this mechanism the cross flow can reattach to the surface $1.6D$ downstream of the hole and may produce instantaneous hot spots on the wall. In the P case the reaction positive vortex is very rare.

To measure the shedding frequency the PIV signal, from a small area through which the positive vortex travels, is transferred to the time signal. If this time signal is transferred into a frequency domain by means of fast Fourier transformation we get the WV shedding frequency of 1 Hz. This frequency is not dependent on the VR. The vorticity time signal shows that vorticity decreases with the velocity ratio in the IT cases but also manifests the insignificant vorticity at the windward side in the P cases.

To examine an averaged time behavior of WVs local maximums of time signal are detected. The measurement fields that contain these maximums are joint to an assemblage. Averaging over such an assemblage leads to a conditional average. WVs are detected and tracked in space and time. The vortices are smaller in IT2 than in IT1 but the maximum vorticity is almost the same. WVs dissipate faster in IT2. The vortices originated from the hole have the opposite sign than the vortices, which would be generated by the Kelvin–Helmholz instability. This can mean that the Kelvin–Helmholz instability accelerates the dissipation of WVs. The velocity difference between the jet and cross flow is higher in IT2 than in IT1. Therefore, the vortices are faster dissipated in IT2. In the conditional averaged fields only the positive vortices are found. If the positive and negative vortex would be a part of one three dimensional vortex then in the conditional averaged figure two vortices should be detected. Since this is not the case we conclude that the toroidal vortex is really broken and the PV and negative vortex that merge later are not part of one whole three dimensional vortex.

In Fig. 8 horizontal instantaneous measurements $0.5D$ above the plate in IT1 are given. Peterson and Plesniak (2002) detected a vortex pair behind the hole which they call downstream spiral separation nodes. Indeed these vortices are detected in the mean flow but from the instantaneous horizontal flow fields it is obvious that they are a periodic vortex pair. In Fig. 8(a) a vortex pair is detected. A few moments later the flow field becomes calm and no vortices can be seen (see Fig. 8(b)). The frequency of these two vortices is also 1 Hz.

In the IT case the jet hole is blocked periodically and the jet is pushed down with the frequency of 1 Hz. A logical attempt would be to connect the vortex pair from the horizontal measurements and the oscillation of the jet. On the basis of the two dimensional experiments in the vertical and horizontal plane we try to make a reconstruction of the three dimensional flow field. A possible scenario can be: the WV leaves the hole and sheds the first shear layer. The LV rolls up on the lee side. At a certain moment it lifts. During the lift the LV passes between the CVP. When the LV goes through the CVP it is stretched and folded. On the top of the first shear layer the WV and LV merge.

4.3. Liquid crystal thermography

The large vortical structures influence the film cooling effectiveness (η). In this section we analyse the η and the effect of the counter rotating vortex pair (CVP), windward (WV) and leeward (LV) vortices on it. Fig. 9(A) presents instantaneous film effectiveness for the P and IT cases at three different velocity ratios. The contact between the cooled volume and the plate wall is called the cooled

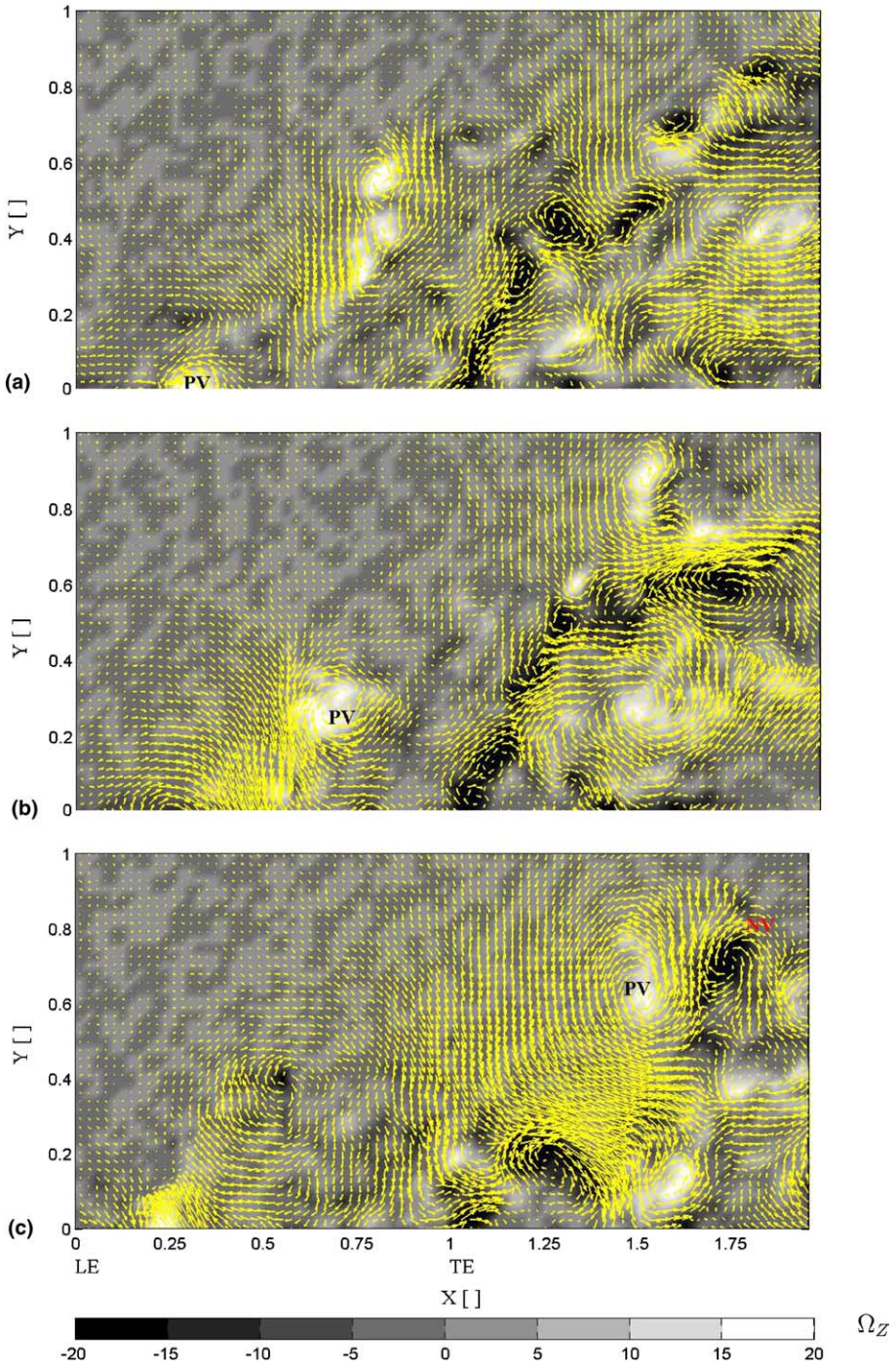

Fig. 6. Fluctuation fields in the IT1 case: (a) At $t = t_0$ PV leaves the hole; (b) at $t = t_0 + 0.33s$ PV sheds the first shear layer; (c) at $t = t_0 + 0.6s$ PV merges with the negative vortex and positive and negative vortices are advected downstream. The same technique and presentation is used as in Fig. 5.

surface. The cooled surface is the smallest in IT1. The jet has the highest momentum, relatively to the cross flow, in IT1 and penetrates deep into the cross flow. Because of the late attachment the cross flow penetrates the cooled volume just behind the hole. Therefore, the cooled surface is narrow and the η is small $1.6D$ downstream, the region of the $\eta > 0.2$ is narrower than further downstream. Additional mixing occurs when the WV interacts either with the LV or positive vortex from the cooled volume. This mixing reduces the η. In P1 the VR is smaller and the momentum, too. The jet attaches better to the surface and the η is increased. In IT2 and P1 the VR is approximately the same but the effectiveness is higher in IT2. In IT2 the jet is pushed down by the stronger cross flow and the expansion after the hole imperfection has the same effect as a shaped hole which enables better reattachment. This produces the higher η in IT2 than in P1 behind the hole. In the far field the effectiveness is similar for both cases. The WVs are smaller and

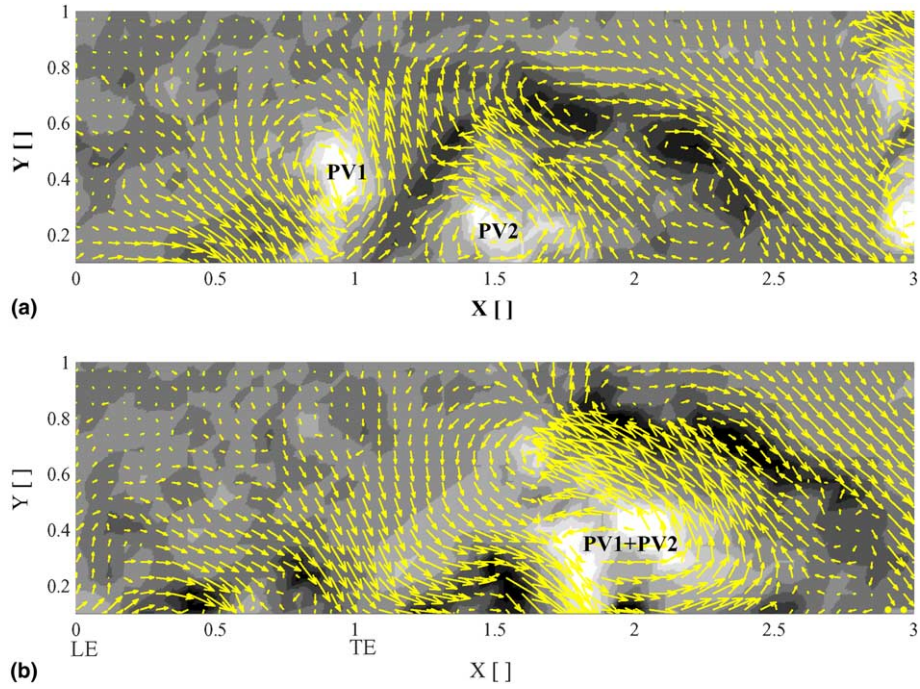

Fig. 7. The instantaneous flow field in the IT2 case. (a) At $t = t_0$ the WV (PV1) sheds the first shear layer, while the positive vortex (PV2) grows till it reaches the length scale of the cooled volume. (b) At $t = t_0 + 0.26s$ the WV merges with the positive vortex and the cross flow reattaches to the plate wall. In figure the fluctuation velocity is plotted and vorticity is given in the background.

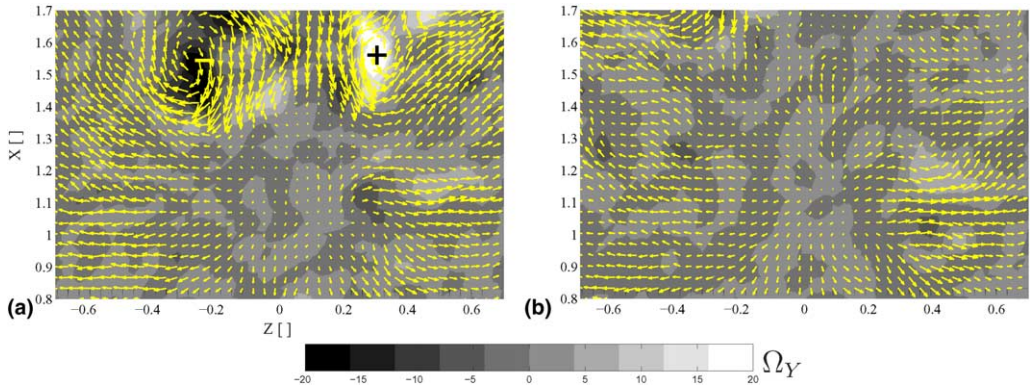

Fig. 8. Horizontal fluctuation fields in IT1. (a) An instantaneous vortex pair in a horizontal plane, (b) An instantaneous horizontal field without vortical structures. A fluctuation velocity and vorticity is shown in the background.

weaker in IT2 than in IT1 so they do not have such a significant influence on the near field as they have in IT1. In the far field the dominant vortical structure is the CVP. The CVP increases the mixing and equalizes the η. In P2 the VR = 0.34 reaches the optimal point for the film cooling process of the perpendicular jet. The cooled surface is large, and the η is continuously distributed. With a further decrease of the VR the inflow below the jet is absent and the cooling improves in the near field but in the far field it is not changed. In IT3 the cooled surface is the same as in P2. The η in the near field is higher but in the far field drops faster in IT3 than in P2 although the VR is the same. The shaped hole improves the attachment and reduces the inflow of a hot fluid towards the central plane which gives a little better η than in P2. But a much more disturbed flow field in the IT cases increases the momentum and heat exchange and decrease the η more rapidly than in the P cases.

Next, the film effectiveness is spanwise averaged (along the Z axis from -0.5 till 0.5) and plotted versus the normalized streamwise (X) coordinate. Results are presented in Fig. 9(B-a). The $\overline{\eta}$ in P1 lies in-between IT1 and IT2 in the near field. In the far field the $\overline{\eta}$ in P1 and IT2 almost match. When the optimal point for the film cooling process of the perpendicular jet is reached, deviations of the $\overline{\eta}$ are rather small in P2, IT3 and P3 in the far field. In the near field an additional push of the jet towards the plate wall improves a little bit the $\overline{\eta}$. In Fig. 9(B-b) central line effectiveness (η_c) is given. The η_c shows similar characteristics as the $\overline{\eta}$. When the VR < 0.34 a further decrease of the VR changes the η_c less than the $\overline{\eta}$. The deviation of the

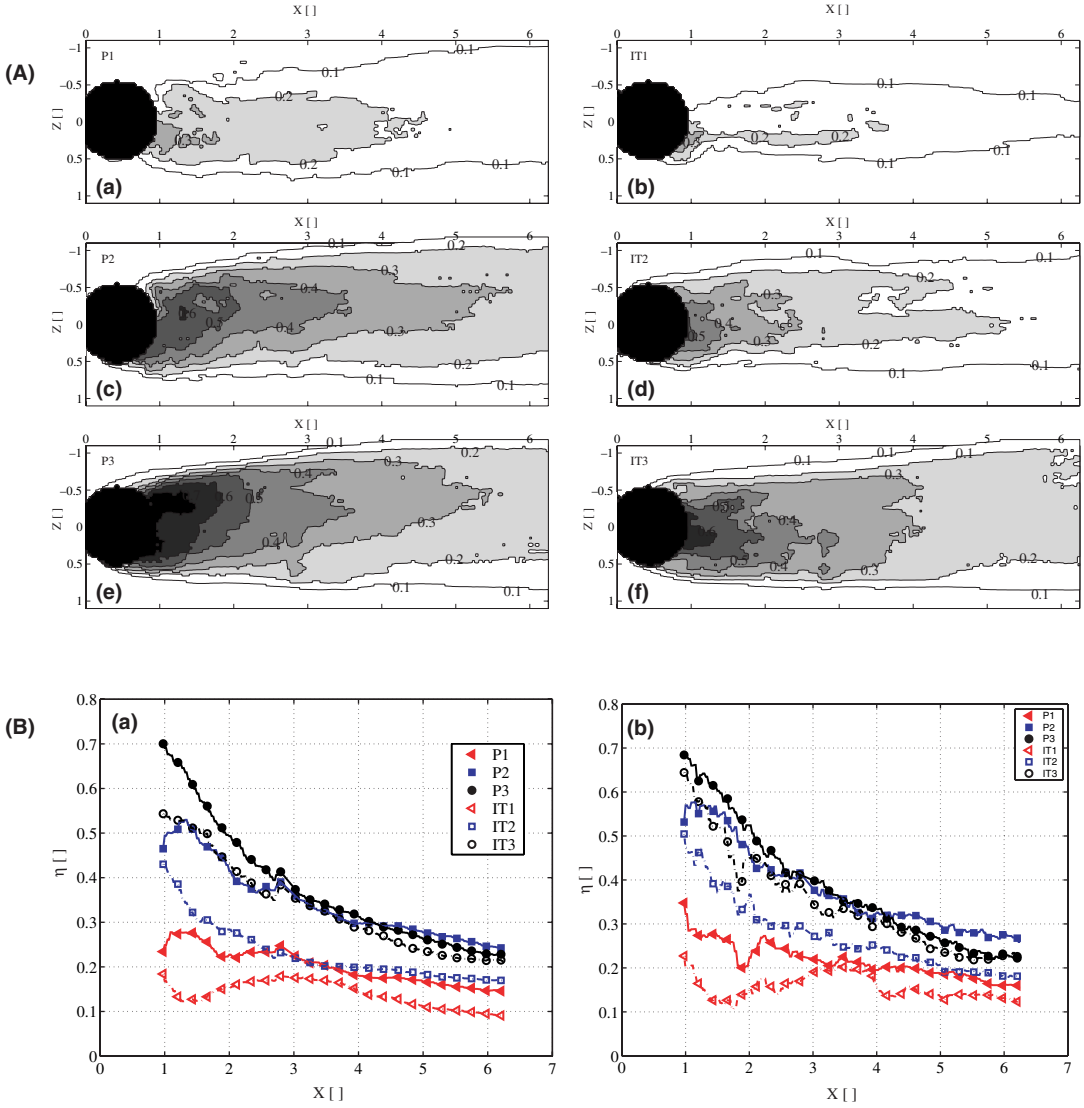

Fig. 9. (A) Instantaneous film cooling effectiveness in: (a) P1, (b) IT1, (c) P2, (d) IT2, (e) P3 and (f) IT3. (B) (a) Lateral averaged film cooling effectiveness, (b) Central line film cooling effectiveness.

effectiveness between the $\overline{\eta}$ and η_c shows that the main heat exchange comes from the side of the hole. Most probably the CVP plays a main role in this process. Therefore, the CVP will be investigated in details in the future work.

5. Conclusions

In this paper the influence of the production imperfection on the flow field and film cooling effectiveness was studied. The perfect hole, hole without imperfection, and the inner-torus hole, hole with the imperfection, are compared. It was found that the imperfection has a large influence on the formation of the large vortical structures and the effectiveness.

From the averaged data it is concluded that the cross flow penetrates the hole much deeper in the IT than in P cases. In the P cases, the ingestion of the cross flow is independent of the velocity ratio, whereas for the IT cases it depends on the velocity ratio. For the velocity ratios larger than 0.5 the penetration of the cross flow towards the central plane and plate surface is significant. This inflow decreases the film cooling effectiveness.

The turbulence intensity above the hole is in the IT case as twice as in P cases and exceeds 30%. Downstream of the hole, the high Tu level concentrates in the second shear layer region in the P case. In the IT case the high Tu spreads across the whole cooled volume.

The large vortical structures are the most responsible for the momentum and heat exchange between the jet and cross flow. It is found that the imperfection has a significant influence on the formation of the vortical structures. In the P case only negative vortices are found leeward. The formation of positive vortices at the lee side is seldom. The presence of the inner-torus in the hole changes the flow field and the vortex roll. Upstream, the windward vortices are detected. The lee vortices are generated downstream. They originate from the torus vortex but out of the hole they form two new structures. The jet oscillates with a fre-

quency of 1 Hz. The shedding frequency of the windward vortices is the same. The windward vortex sheds the first shear layer and merges with the lee vortex. Another scenario occurs in the IT case. If the positive vortex rolls up in the cooled volume then the windward vortex pairs up with it, deteriorates the flow field and the cross flow reattaches to the plate surface in the vicinity of the hole. This reattachment can produce a hot spot on a blade surface in gas turbines.

The windward and lee vortices influence the effectiveness in the vicinity of the hole. The mechanism, described earlier, decreases the film cooling effectiveness in the inner torus case for the velocity ratio larger than 0.5. When the velocity ratio drops below 0.35 the optimal point for transversal film cooling is reached and the inner-torus has an influence in the near field but it does not influence the film cooling performances in the far field.

References

Adrian, R.J., Christensen, K.T., Liu, Z.-C., 2000. Analysis and interpretation of instantaneous turbulent velocity fields. Exp. Fluids 29, 275–290.

van Allmen, M., Blatter, A., 1995. Laser–Beam Interaction with Metal. Springer-Verlag, pp. 115–134.

Andreopoulos, J., 1982. Measurements in a jet-pipe flow issuing perpendicularly into a cross stream. ASME J. Fluid Engine 104, 493–499.

Andreopoulos, J., Rodi, W., 1984. Experimental investigation of jets in a crossflow. J. Fluid Mech. 138, 93–127.

Bergeles, G., Gosman, A.D., Launder, B.E., 1976. The near-field character of a jet discharged normal to a main stream. ASME J. Heat Transfer, 373–379.

Fric, T.F., Roshko, A., 1994. Vortical structure in the wake of a transverse jet. J. Fluid Mech. 279, 1–47.

Gritsch, M., Schultz, A., Witting, S., 1998. Discharge coefficient measurements of film cooling holes with expanded exits. ASME J. Turbomach. 120, 557–563.

Haven, B.A., Kurosaka, M., 1997. Kidney and anti-kidney vortices in crossflow jets. J. Fluid Mech. 352, 27–64.

Hay, N., Lampard, D., Saluja, C.L., 1985. Effects of the condition of the approach boundary layer and of mainstream pressure gradients on the heat transfer coefficient on film-cooled surfaces. J. Engine Gas Turb. Power 107, 99–104.

Johnston, J.P., Mosier, B.P., Khan, Z.U., 2002. Vortex generating jets effects of jet-hole inlet geometry. Int. J. Heat Fluid Flow 23, 744–749.

Kelso, R.M., Lim, T.T., Perry, A.E., 1996. An experimental study of round jets in cross flow. J. Fluid Mech. 306, 111–114.

Lim, T.T., New, T.H., Luo, S.C., 2001. On the development of large-scale structures of a jet normal to a cross flow. Phys. Fluids 13 (3), 770–775.

Lourenco, L., Subramanian, S., Ding, Z., 1997. Time series velocity field reconstruction from PIV data. Meas. Sci. Technol. 8, 1533–1538.

Morton, B.R., Ibbetson, A., 1996. Jets deflected in a crossflow. Exp. Therm. Fluid Sci. 12, 112–133.

Moussa, Z.M., Trischka, W.J., Eskinazi, S., 1997. The near field of the mixing of a round jet in cross-stream. J. Fluid Mech. 80, 49–80.

New, T.H., Lim, T.T., Luo, S.C., 2003. Elliptic jets in cross flow. J. Fluid Mech. 494, 119–140.

Peterson, S.D., Plesniak, M.W., 2002. Short-hole jet-in-crossflow velocity field and its relationship to film-cooling performance. Exp. Fluids 33, 889–898.

van der Plas, G.A.J., Bastiaans, R.J.M., 1998. Accuracy and resolution of the fast PTV algorithm suitable for HiRes-PV. In: Carlomagno, G.M., Grant, I., (Eds.), Proceedings of 8th International Symposium of Flow Visualization. ISBN 0953399709, paper 87.

Schook, R., de Lange, H.C., van Steenhoven, A.A., 2001. Unsteady heat transfer in subsonic boundary layers. Int. J. Heat Fluid Flow 22, 272–278.

Smith, S.H., Mungal, M.G., 1998. Mixing, structure and scaling of the jet in crossflow. J. Fluid Mech. 357, 83–122.

Yuan, L.L., Street, R.L., Ferziger, J.H., 1999. Large-eddy simulation of a round jet in crossflow. J. Fluid Mech. 379, 71–104.